Title: CDKG1 Is Required for Meiotic and Somatic Recombination Intermediate Processing in Arabidopsis

Author: Candida Nibau, Andrew Lloyd, Despoina Dadarou, Alexander Betekhtin, Foteini Tsilimigka, Dylan W. Phillips, John H. Doonan

Citation style: Nibau Candida, Lloyd Andrew, Dadarou Despoina, Betekhtin Alexander, Tsilimigka Foteini, Phillips Dylan W., Doonan John H. (2020). CDKG1 Is Required for Meiotic and Somatic Recombination Intermediate Processing in Arabidopsis. "The Plant Cell" Vol. 32, iss. 4 (2020), s. 1308-1322, doi 10.1105/tpc.19.00942

The Plant Cell, Vol. 32: 1308–1322, April 2020, www.plantcell.org © 2020 ASPB.

CDKG1 Is Required for Meiotic and Somatic Recombination Intermediate Processing in Arabidopsis[CC-BY]

Candida Nibau,[a,1] Andrew Lloyd,[a] Despoina Dadarou,[a,2] Alexander Betekhtin,[b] Foteini Tsilimigka,[a] Dylan W. Phillips,[a] and John H. Doonan[a,1]

[a] Institute of Biological, Rural and Environmental Sciences, Aberystwyth University, Gogerddan, Aberystwyth SY23 3EB, United Kingdom

[b] Institute of Biology, Biotechnology and Environmental Protection, Faculty of Natural Sciences, University of Silesia in Katowice, Katowice 40-007, Poland

ORCID IDs: 0000-0002-0877-6001 (C.N.); 0000-0001-7871-6621 (A.L.); 0000-0001-7031-3342 (D.D.); 0000-0001-6146-1669 (A.B.); 0000-0001-9977-7562 (F.T.); 0000-0002-9139-5727 (D.W.P.); 0000-0001-6027-1919 (J.H.D.)

The Arabidopsis (*Arabidopsis thaliana*) cyclin-dependent kinase G1 (CDKG1) is necessary for recombination and synapsis during male meiosis at high ambient temperature. In the *cdkg1-1* mutant, synapsis is impaired and there is a dramatic reduction in the number of class I crossovers, resulting in univalents at metaphase I and pollen sterility. Here, we demonstrate that CDKG1 is necessary for the processing of recombination intermediates in the canonical ZMM recombination pathway and that loss of CDKG1 results in increased class II crossovers. While synapsis and events associated with class I crossovers are severely compromised in a *cdkg1-1* mutant, they can be restored by increasing the number of recombination intermediates in the double *cdkg1-1 fancm-1* mutant. Despite this, recombination intermediates are not correctly resolved, leading to the formation of chromosome aggregates at metaphase I. Our results show that CDKG1 acts early in the recombination process and is necessary to stabilize recombination intermediates. Finally, we show that the effect on recombination is not restricted to meiosis and that CDKG1 is also required for normal levels of DNA damage-induced homologous recombination in somatic tissues.

INTRODUCTION

During sexual reproduction, the genomic complement of diploid cells is halved by a highly specialized nuclear division, called meiosis, to produce haploid gametes. In meiotic prophase I, homologous chromosomes pair, synapse, and recombine. These three processes are intimately linked, and defects in any one often lead to reduced fertility due to nondisjunction. Meiotic prophase I is divided into five substages: leptotene, zygotene, pachytene, diplotene, and diakinesis. During leptotene, recombination is initiated by the formation of double strand breaks (DSBs) catalyzed by the highly conserved topoisomerase Sporulation-deficient11 (SPO11), followed by the invasion of single strand DSB ends into homologous sequences, creating a D-loop mediated by the recombinases Disrupted Meiotic cDNA1 (DMC1) and Radiation sensitive51 (RAD51; Bishop et al., 1992; Sung and Robberson, 1995; Keeney et al., 1997). Following D-loop formation, recombination-associated DNA synthesis occurs using the complementary strand of the invaded duplex as a template. If the D-loops are extended, they can give rise to a unique heteroduplex DNA configuration called a double Holliday junction. The mode of resolution of this joint molecule determines the outcome either as a crossover (CO) or as a noncrossover (NCO; Allers and Lichten, 2001).

The resolution of stabilized double Holliday junctions into COs is dependent on the activity of ZMM proteins including MutS homologue4 (MSH4), MSH5, and Human Enhancer of Invasion10 (HEI10; Higgins et al., 2004, 2008b; Chelysheva et al., 2012). These ZMM proteins are responsible for the formation of interference-sensitive class I COs that account for 80 to 90% of meiotic COs (Basu-Roy et al., 2013). A number of additional pathways repair DSBs that are not metabolized by the ZMM proteins. In most cases, these DSB repair pathways resolve joint molecules as NCOs, but they also contribute a small number of COs, mostly mediated by either MMS and UV sensitive81 (MUS81; Berchowitz et al., 2007; Higgins et al., 2008a) or Fanconi anemia D2 (FANCD2; Kurzbauer et al., 2018). These class II COs are insensitive to interference and usually make up 10 to 20% of the total CO number (Housworth and Stahl, 2003; Basu-Roy et al., 2013).

In Arabidopsis (*Arabidopsis thaliana*), between ~150 and 250 DSBs are formed, but only ~10 are processed as COs (Mercier et al., 2015). The rest are processed as NCOs via synthesis-dependent strand annealing, dissolution of joint molecules, or by other mechanisms. This implies that there are mechanisms designating which DSBs become resolved as COs and that there are inhibitory mechanisms preventing resolution of DSBs into COs at the remaining sites. While the factors involved in CO designation remain elusive, recent studies have identified anti-CO factors that include the DNA helicases RECQ4A and RECQ4B, Topoisomerase3α, RECQ Mediated Genome Instability1 (RMI), the

[1] Address correspondence to csn@aber.ac.uk and john.doonan@aber.ac.uk.

[2] Current address: School of Life Sciences, University of Warwick, Coventry, CV4 7AL, United Kingdom

The authors responsible for distribution of materials integral to the findings presented in this article in accordance with the policy described in the Instructions for Authors (www.plantcell.org) are: Candida Nibau (csn@aber.ac.uk) and John H. Doonan (john.doonan@aber.ac.uk).

www.plantcell.org/cgi/doi/10.1105/tpc.19.00942

IN A NUTSHELL

Background: Cyclin-dependent kinases are involved in many cellular processes ranging from external signal perception, division and death. Our work has shown that CDKG1 is necessary for the correct progression of meiosis, a specialised form of cell division that results in gamete production. During meiosis, both sets of parental chromosomes find each other, pair and reciprocally exchange DNA in a process called recombination, before correctly segregating into the daughter cells. In plants lacking CDKG1, the first steps of the recombination process progress normally but the parental chromosomes fail to fully pair and reduced numbers of mature recombination molecules are observed. This results in incorrect chromosome segregation, unbalanced gametes and sterility.

Question: In this study we delve deeper into the meiotic role of the CDKG1 kinase and reveal how it interacts with other known meiotic functions to achieve an orderly reduction division.

Findings: In Arabidopsis, most meiotic recombination (~85%) occurs via the major class I pathway, with a smaller contribution (~15%) by the minor class II pathway(s). We demonstrate that CDKG1 is necessary for regular processing of recombination precursors by the class I pathway. In the absence of CDKG1, fewer early precursors of class I recombination persist and there is an increase in recombination events occurring via the class II pathway. Using a genetic approach, we further increased levels of class II recombination, which restored chromosome pairing, synapsis and class I recombination in the *cdkg1* mutant. We suggest that CDKG1 acts early in the meiotic DNA repair process to stabilise recombination precursors so they can be effectively processed by the class I recombination machinery. In addition, we show that CDKG1 is also involved in somatic DNA repair.

Next steps: We now want to investigate the mechanism by which the CDKG1 kinase stabilises recombination precursors. Does it physically associate with recombination sites? Does it phosphorylate other meiotic proteins? Or, does it act by regulating the abundance of meiotic proteins through post-transcriptional or post-translational regulatory mechanisms?

DNA helicase FANCM and its cofactors MHF1 and MFH2 (FANCM interacting histone-fold protein), and the AAA-ATPase Fidgetin-like1 (FIGL1) and its interacting protein *FIDGETIN*-LIKE-1 INTERACTING PROTEIN (FLIP; Crismani et al., 2012; Dangel et al., 2014; Girard et al., 2014, 2015; Seguela-Arnaud et al., 2015, 2017; Fernandes et al., 2018; Kurzbauer et al., 2018; Serra et al., 2018).

The DNA helicase FANCM was first identified in Arabidopsis in a reverse genetic screen for factors suppressing CO formation (Crismani et al., 2012). In humans, FANCM is a core component of the Fanconi Anemia network that preserves genome stability by promoting the resolution of inter-strand cross-links (Kottemann and Smogorzewska, 2013). The FANCM protein contains an N-terminal helicase domain and a C-terminal nuclease domain (Whitby, 2010). The helicase activity is necessary for its role as an anti-CO protein as mutations in conserved residues within the helicase domain increase CO formation (Crismani et al., 2012). In Arabidopsis, the absence of FANCM increases CO frequency by threefold, and the extra COs are formed by the MUS81-dependent class II pathway (Crismani et al., 2012). In an independent study, FANCM was also found to be required for DSB-induced somatic homologous recombination (HR; Knoll et al., 2012). It was proposed that FANCM acts by unwinding the D-loop recombination intermediates and channelling them through an NCO pathway. In the absence of FANCM, these recombination intermediates would be processed through the class II recombination pathway. This implies that the recombination sites on which FANCM acts are distinct from those processed by the ZMM-dependent class I pathway.

Concomitant with the recombination process is the formation of the synaptonemal complex (SC). SC formation is initiated early in meiosis between homologous chromosomes. The axial element proteins Asynaptic1 (ASY1), REC8, and ASY3 form a protein axis where the chromatin loops from sister chromatids are anchored in linear arrays (Mercier et al., 2015; Lambing et al., 2017). The central element protein ZYP1 polymerizes between the tracks of axial element proteins, spatially aligning the homologous chromosomes in close register. After CO formation is complete, the SC dissociates and homologous chromosomes are kept together at CO sites.

There is a close interaction between SC formation and CO designation, but how this interaction happens and which proteins are involved remains unclear. Several observations suggest that recombination and SC formation are tightly linked. In most organisms, including Arabidopsis, SC formation is dependent on DSB formation and strand invasion as *atspo11-1*, *atrad51-1*, and *dmc1* mutants defective in DSB formation or repair fail to synapse (Couteau et al., 1999; Li et al., 2004). Additionally, in some organisms, the number of SC initiation sites (SICs) is directly related with the number of late recombination nodules (Gray and Cohen, 2016). Finally, central element proteins have been shown to have a role in CO formation (Colaiácovo et al., 2003; Jang et al., 2003; Couteau et al., 2004; Zickler, 2006). Interestingly, unlike in other species, Arabidopsis ZMM proteins are not necessary for SC formation (Higgins et al., 2004, 2005, 2008b), indicating that once strand invasion has occurred SC polymerization can progress.

Although many of the components of the recombination and pairing machinery have been identified, their specific role and those of other associated molecules in these processes is not yet fully understood. One of those components is the cyclin-dependent kinase G1 (CDKG1) that belongs to the same kinase group as mammalian CDK10/11 (Doonan and Kitsios, 2009). CDKG1 is also related to the kinases present in the *Ph1* locus in wheat (*Triticum aestivum*) that controls pairing and recombination between homologous chromosomes (Greer et al., 2012), and we

previously showed that CDKG1 was necessary for normal levels of COs and synapsis in male meiosis at high ambient temperature (Zheng et al., 2014). While the formation of DSBs was not affected in the *cdkg1-1* loss-of-function mutant, the number of COs was drastically reduced, causing plant sterility. In addition, loading of the axial elements of the SC was normal, but the polymerization of the central element protein ZYP1 was reduced in the *cdkg1-1* mutant. As ZMM mutants undergo full synapsis (Higgins et al., 2004, 2008b; Mercier et al., 2005; Chelysheva et al., 2012; Wang et al., 2012), it is possible that CDKG1 acts upstream of the ZMM proteins.

To address how CDKG1 affects recombination and synapsis, we examined the genetic interactions between *cdkg1-1* and a variety of mutants that have characterized defects in different stages of the CO determination and formation process. We show that, while synapsis is severely compromised in a *cdkg1-1* mutant, it is restored by increasing the number of recombination intermediates in a double *cdkg1-1 fancm-1* mutant. The restoration of synapsis in the double mutant is accompanied by the restoration of the wild-type numbers of HEI10 and MLH1 foci, indicating that synapsis is sufficient for normal class I CO formation in the absence of CDKG1. Thus, we infer that the synapsis defect in the single *cdkg1-1* mutant results from a lack of suitable recombination precursors rather than the recombination defect being due to a lack of synapsis. In addition, the *cdkg1-1* mutation is able to partially rescue the phenotype of the ZMM mutant, *msh5-2*, suggesting that in the absence of CDKG1 early intermediates not resolved by the ZMM proteins are processed by the class II processing pathways. Together, our results indicate that CDKG1 is necessary for the processing of recombination intermediates into the class I CO pathway.

RESULTS

Loss of CDKG1 Increases Class II COs

Our previous work showed that the *cdkg1-1* mutant retains a low level of class I COs (2.5 ± 2.4 per cell; Zheng et al., 2014). To further investigate the role of CDKG in class I DSB repair, the *cdkg1-1* mutant was crossed with the previously described class I CO mutant *msh5-2* (Higgins et al., 2008b). In the *msh5-2* mutant, class I CO formation is compromised and bivalent formation is dramatically reduced (from five bivalents in the wild type Columbia-0 [Col-0] to 1.1 ± 0.99 in the *msh5-2* mutant; Figures 1A and 1B), as was reported previously (Higgins et al., 2008b). The *cdkg1-1 msh5-2* double mutant showed a significant increase in bivalent formation at metaphase I (1.1 ± 0.99 bivalents in the *msh5-2* mutant and 2.5 ± 0.95 in the *cdkg1 msh5-2* double mutant; two-tailed *t* test, $P < 0.001$; Figures 1A and 1B) and a concomitant significant increase in seed set (Figure 1C).

As the class I CO pathway is compromised by the absence of MSH5, the increased bivalent number in the double *cdkg1-1 msh5-2* must be generated by increased class II COs. This suggests that loss of CDKG1 increases class II CO formation. If this were the case, we would also expect to see more class II COs

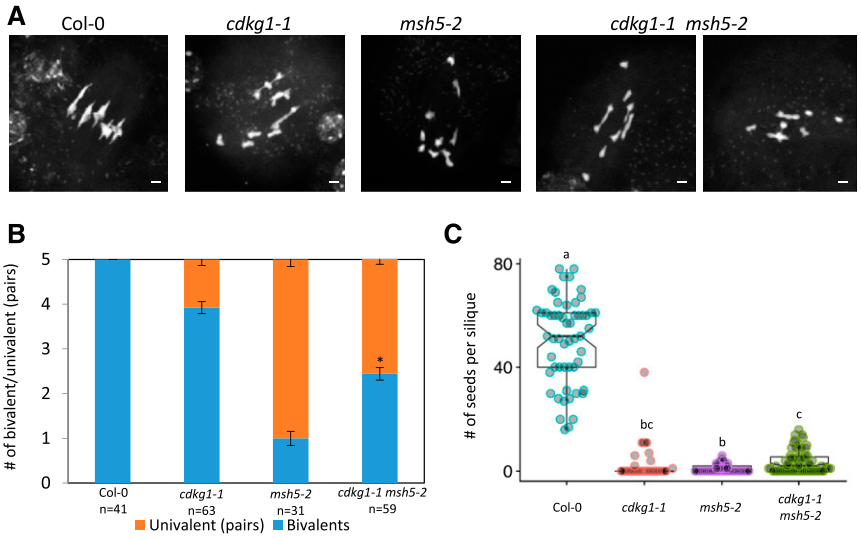

Figure 1. The *cdkg1-1* Mutation Increases Bivalent Formation in the *msh5-2* Mutant Background.

(A) DAPI-stained metaphase I spreads. Bar = 2 μm.

(B) Ratio of bivalent to univalent pairs present at metaphase I. Error bars represent average ± SD, and *n* indicates the number of metaphases counted for each genotype. Asterisk indicates that the bivalent number in the *cdkg1-1 msh5-2* mutant is significantly different from the single *msh5-2* mutant for $P < 0.001$, two-tailed *t* test.

(C) Fertility counts in the wild type (Col-0) and indicated mutants. Graphs show mean and interquartile range as well as the actual seed counts. For each genotype, at least 30 siliques from three independent plants were counted. Superscript letters indicate the significance groups for $P < 0.001$ calculated using ANOVA, with post hoc pairwise *t* tests using nonpooled SD and Bonferroni correction.

in the *cdkg1-1* single mutant compared with Col-0. To further test this possibility, we used a modeling approach to identify the best fit values of class II COs in the three mutant contexts (i.e., *cdkg1-1*, *msh5-2*, and *cdkg1-1 msh5-2*). Specifically, we compared bivalent counts observed experimentally with those observed in simulations where the number of class II COs varied from 0.5 to 7 per meiosis.

For simulations, we used the beam-film model of CO patterning (Zhang et al., 2014; White et al., 2017), with parameter values that were previously determined for the Arabidopsis wild-type male meiosis (Lloyd and Jenczewski, 2019); the class I CO maturation parameter (M) was adjusted to reflect the differing number of class I COs in the respective lines. For *msh5-2*, the best fit value was 1.16 class II COs; the best fit bivalent distribution was identical to that experimentally observed for *msh5-2* but differed significantly from that of the *cdkg1-1 msh5-2* double mutant (Figure 2). For the double *cdkg1-1 msh5-2* mutant the best fit value was 3.41 class II COs per meiosis; the best fit bivalent distribution (3.41 class II COs) was no different from that experimentally observed for *cdkg1-1 msh5-2* (Figure 2) but differed significantly from that observed experimentally for the single *msh5-2* mutant (Figure 2). For the single *cdkg1-1*, the best fit value was 3.76 class II COs per meiosis; the best fit bivalent distribution (3.76 class II COs) was no different from that experimentally observed for *cdkg1-1* (Figure 2) and equivalent to that determined for *cdkg1-1 msh5-2* (Supplemental Figure 1). By contrast, distributions from simulations assuming 1.16 class II COs per meiosis (i.e., the number of class II COs derived from our *msh5-2* observations) differed significantly from bivalent distributions observed for *cdkg1-1* (Figure 2). The same results were obtained assuming 1.5 class II COs per meiosis (Supplemental Table 1), that is, the number of class II COs per meiosis reported in numerous previous studies. Together, these results suggest that loss of CDKG1 results in an approximately threefold increase in the number of class II COs in both the presence and absence of MSH5.

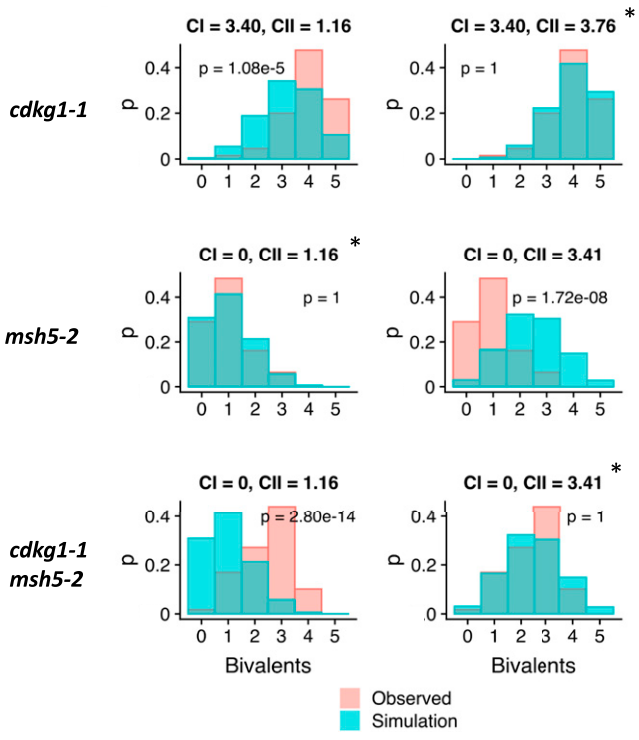

Figure 2. Bivalent Distribution Comparisons for Simulated and Experimentally Observed Meioses.

Bivalent distributions for observed (pink) and simulated (blue) meioses for *cdkg1-1*, *msh5-2*, and *cdkg1-1 msh5-2*. For simulations, the number of class I (CI) COs was fixed based on experimental observations, and the number of class II (CII) COs varied from 0.5 to 7 per meiosis. Bivalent distributions of best fit simulations are shown (*). In addition, bivalent distributions for *cdkg1-1* and *cdkg1-1 msh5-2* are compared with those from simulated meiosis with 1.16 CII COs (the best fit value for *msh5-2*), and the msh5-2 bivalent distribution is compared with simulated meiosis with 3.41 CII COs (the best fit for *cdkg1-1 msh5-2*). P-values are Bonferroni-corrected values derived from two-sample Kolmogorov–Smirnov tests.

The Extra Class II COs Present in the *cdkg1-1* Mutant Are Not MUS81 Dependent

To establish whether the extra COs arise from a MUS81-dependent pathway, we crossed the *cdkg1-1* mutant with the *mus81-2* mutant. While bivalent formation and seed set are normal in the *mus81-2* mutant, the double *cdkg1-1 mus81-2* mutant shows similar bivalent formation and seed set to that observed in the single *cdkg1-1* mutant (Figures 3A to 3C). This decreased bivalent formation is accompanied by reduced numbers of class I COs as detected by the presence of MLH1 foci (Figures 3D and 3E). In the double *cdkg1-1 mus81-2* mutant, the number of MLH1 foci is reduced to levels comparable to that of the single *cdkg1-1* mutant (2.7 ± 2.3 in *cdkg1-1*, $n = 30$ and 3.6 ± 2.7 in *cdkg1-1 mus81-2*, $n = 31$; $P = 1$ ANOVA, post hoc pairwise *t* test with nonpooled SD and Bonferroni correction; Figures 3D and 3E), while the single *mus81-2* mutant has the wild-type levels of class I COs (9.75 ± 2.03, $n = 20$ in Col-0 and 10.1 ± 1.9, $n = 15$ in *mus81-2*; $P = 1$, ANOVA, post hoc pairwise *t* test with nonpooled SD and Bonferroni correction; Figures 3D and 3E).

Synapsis is also defective in the double *cdkg1-1mus81-2* mutant. At pachytene, in both Col-0 and the *mus81-2* mutant, full synapsis is observed with all the homologous chromosomes paired and a continuous signal of the central element protein ZYP1 being observed along the chromosome axis (Figure 3E). In both the single *cdkg1-1* mutant and the double *cdkg1-1 mus81-2* mutant, synapsis is impaired (Figure 3E). As the double *cdkg1-1 mus81-2* mutant forms the same number of bivalents as the single *cdkg1-1* mutant, we conclude that the extra class II COs are formed through a MUS81-independent pathway.

Synapsis and CO Formation Are Restored in the *cdkg1-1 fancm-1* Double Mutant

From the ~100 DSBs that enter the class II pathways, the majority are processed into NCOs by the activity of anti-recombinases (Mercier et al., 2015). One of these is the helicase FANCM that directs these recombination intermediates toward NCO repair or sister chromatid events. To determine the interaction between CDKG1 and the NCO pathways, we crossed the *cdkg1-1* mutant

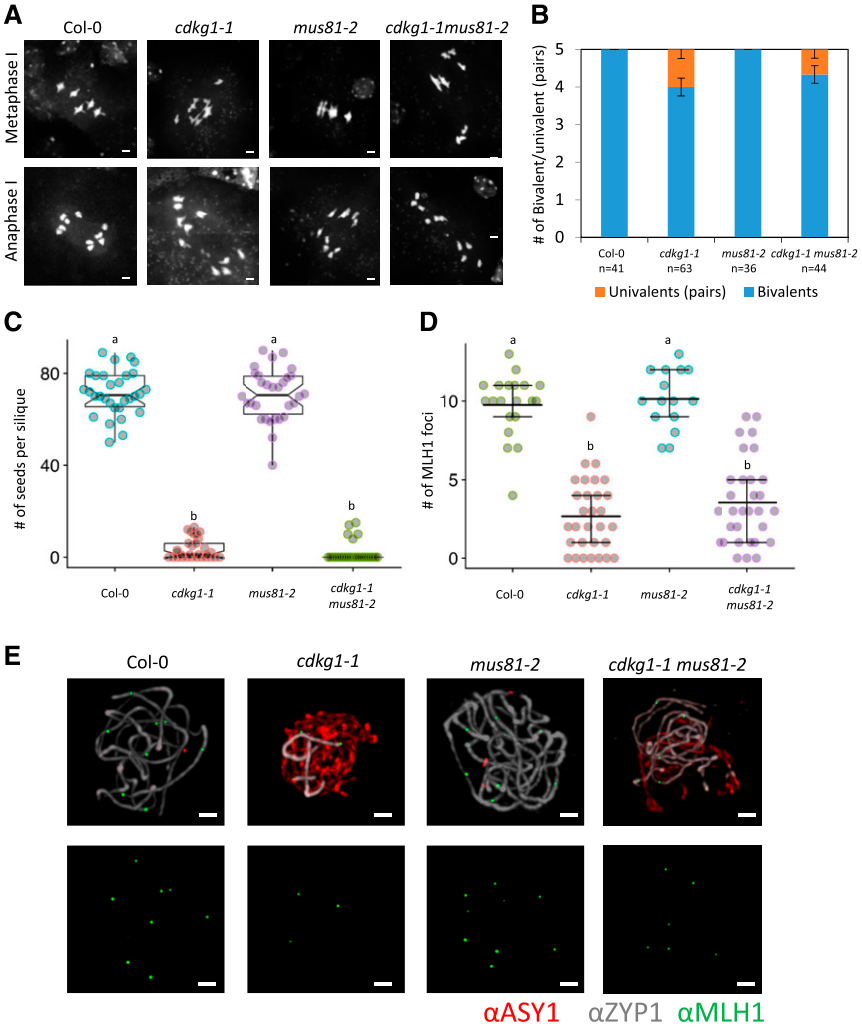

Figure 3. The Meiotic Phenotype of the Double *cdkg1-1 mus81-2* Mutant Is Similar to the Single *cdkg1-1* Mutant.

(A) DAPI-stained metaphase I spreads of the indicated mutants. Bar = 2 μm.
(B) Ratio of bivalent to univalent pairs present at metaphase I. Error bars represent average ± SD, and *n* indicates the number of metaphases counted for each genotype.
(C) Fertility counts in the indicated mutants. Graphs show mean and interquartile range as well as the actual seed counts. For each genotype at least 30 siliques from three independent plants were counted. Superscript letters indicate the significance groups for $P < 0.001$ calculated using ANOVA, with post hoc pairwise *t* tests using nonpooled SD and Bonferroni correction.
(D) Number of MLH1 foci observed in the indicated mutants. Graphs show mean and interquartile range as well as the actual foci counts. Superscript letters indicate the significance groups for $P < 0.001$ calculated using ANOVA, with post hoc pairwise *t* tests using nonpooled SD and Bonferroni correction.
(E) Immunolocalization of the class I CO marker protein MLH1 in the indicated mutants. The axial element protein ASY1 is labeled in red, the central element protein ZYP1 in gray, and MLH1 foci in green (top panels). The MLH1 channel (green) is also shown separately (bottom panels). Images represent maximum projections of Z-stacks. Bar = 2 μm.

with the well-described *fancm-1* mutant and examined homologous chromosome pairing and CO formation in the double *cdkg1-1 fancm-1* mutant.

In Col-0 and single *fancm-1* mutant cells at pachytene, full homologous chromosome synapsis is observed as determined by ZYP1 loading (Figure 4A). In the single *cdkg1-1* mutant, as we have reported previously (Zheng et al., 2014), ZYP1 loading is dramatically reduced (Figure 4A) and the five bivalents fail to fully synapse (Figures 4A and 4B). Strikingly, in the double *cdkg1-1 fancm-1* mutant, synapsis is fully restored (Figure 4A), and five nearly fully synapsed bivalents can be computationally isolated (Figure 4B). Using the presence of ASY1 to measure the total SC length and ZYP1 to quantify the synapsed regions, we calculated that in the *cdkg1-1 fancm-1* double mutant the average synapsis is 96% (range, 71 to 100%; SD = 0.075; *n* = 10 cells). The average synapsis previously reported for the single *cdkg1-1* mutant is

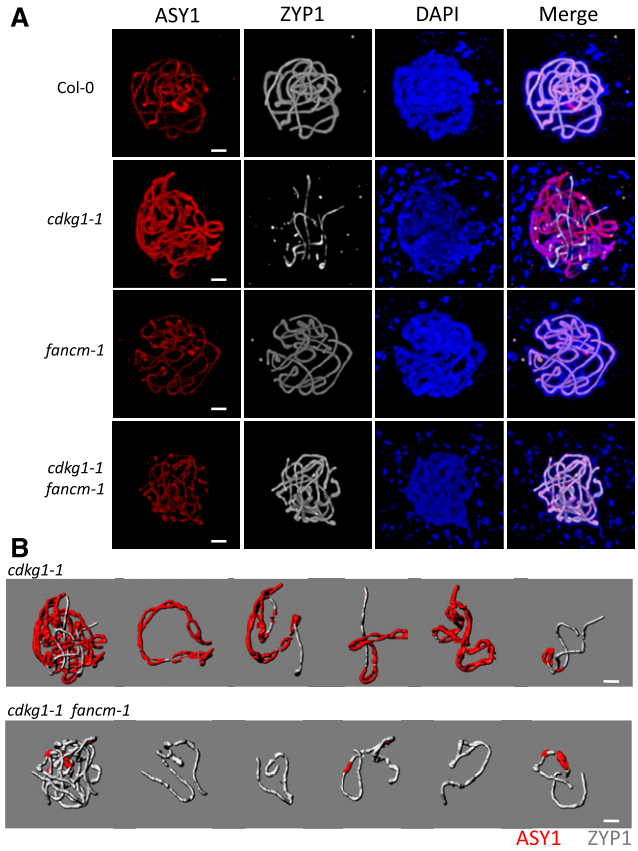

Figure 4. Chromosome Synapsis Is Restored in the *cdkg1-1 fancm-1* Double Mutant.

(A) Immunolocalization of the axial element protein ASY1 (red) and the central element protein ZYP1 (gray) in pachytene nuclei of Col-0, *cdkg1-1*, *fancm-1*, and *cdkg-1-1 fancm-1* mutant plants. DNA is counterstained with DAPI (blue), and a merge of all channels is shown. Images represent maximum projections of Z-stacks. Bar = 2 μm.

(B) Three-dimensional reconstruction of a whole nucleus and individual bivalents from a *cdkg1-1* pachytene-like nucleus and a *cdkg1-1 fancm-1* pachytene nucleus. The nuclei were processed using Imaris software, and each bivalent pair was isolated and false colored. Unpaired regions are marked by the presence of ASY1 (red) and paired regions by the presence of ZYP1 (gray). Bar = 2 μm.

29.92% (range, 0 to 73.76%; SD = 0.185; $n = 10$ cells), showing that in the absence of both CDKG1 and FANCM, ZYP1 is able to load onto the chromosome axis at normal levels.

This observation could be explained by restoration of ZMM-associated synaptic initiation complexes in the double *cdkg1-1 fancm-1* mutant or if the additional class II recombination intermediates (introduced by the *fancm-1* mutation) are able to initiate synapsis. To distinguish between these two possibilities, we determined the localization of ZMM proteins MLH1 and HEI10.

In late pachytene, the MLH1 protein localizes to mature recombination sites, and the number of MLH1 foci observed corresponds to the number of class I COs. In the *fancm-1* mutant, we observe the wild-type levels of MLH1 foci (10.14 ± 1.87, $n = 7$ in Col-0 and 11.42 ± 2.43, $n = 19$ in *fancm-1*; P = 1, ANOVA, post hoc pairwise *t* test with nonpooled SD and Bonferroni correction), while in the *cdkg1-1* drastically reduced numbers of MLH1 foci were observed (4.61 ± 1.5, $n = 18$; $P < 0.001$, ANOVA, post hoc pairwise *t* test with nonpooled SD and Bonferroni correction), as previously described by Zheng et al. (2014; Figures 5A and 5B). Interestingly, in the *cdkg1-1 fancm-1* double mutant, we observed the wild-type levels of MLH1 (9.62 ± 2.82, $n = 13$; P = 1, ANOVA, post hoc pairwise *t* test with nonpooled SD and Bonferroni correction; Figures 5A and 5B). These data suggest that the presence of an increased number of recombination intermediates caused by the absence of FANCM is sufficient to restore class I CO-associated events.

Similar results were observed for HEI10 localization in late pachytene and diplotene cells. While the *cdkg1-1* single mutant has fewer HEI10 foci, the wild-type levels are restored in the double *cdkg1-1 fancm-1* mutant (Col-0: 9.9 ± 0.64, $n = 7$; *cdkg1-1*: 3.41 ± 1.91*, $n = 17$; *fancm-1*, 11.17 ± 1.5, $n = 6$; *cdkg1-1 fancm-1*, 9.9 ± 1.92, $n = 10$; *$P < 0.001$, ANOVA, post hoc pairwise *t* test with nonpooled SD and Bonferroni correction; Figures 5A and 5C). Besides marking mature class I CO sites later in meiosis, the ZMM protein HEI10 also marks early recombination intermediates in leptotene/zygotene (Chelysheva et al., 2012). We observed a reduced number of HEI10 foci in *cdkg1-1* in leptotene and early zygotene cells (Col-0: 76 ± 11.01, $n = 5$; *cdkg1-1*: 21.58 ± 12.09, $n = 12$; $P < 0.001$, ANOVA, post hoc pairwise *t* test with nonpooled SD and Bonferroni correction), indicating that fewer class I recombination intermediates are present in this mutant, but this defect is restored in a *cdkg1-1 fancm-1* double mutant (*cdkg1-1 fancm-1*: 67.11 ± 22.61, $n = 9$; P = 1; ANOVA, post hoc pairwise *t* test with nonpooled SD and Bonferroni correction; Supplemental Figure 2).

In addition, under our immunolocalization conditions and as seen by others (Hurel et al., 2018; Li et al., 2018), HEI10 also localizes to synapsed chromosome axes, emphasizing that the partial synapsis observed in a single *cdkg1-1* mutant is restored in a *cdkg1-1fancm-1* double mutant (Supplemental Figure 2).

Taken together, these data suggest that the increased number of ZMM-bound early recombination intermediates in the double *cdkg1-1 fancm-1* mutant are able to restore synapsis and class I CO defects caused by the absence of CDKG1.

Recombination Intermediates Are Not Correctly Resolved in the *cdkg1-1 fancm-1* Double Mutant

Although synapsis is restored in a *cdkg1-1 fancm-1* double mutant, meiotic defects appear in late prophase. In the single *fancm-1* mutant, full synapsis was observed at pachytene, five bivalents observed at metaphase I, and four meiotic products with five chromosomes each observed at telophase II (Figure 6A). In the *cdkg1-1 fancm-1* double mutant, synapsis progressed normally, but chromosome aggregates (without fragmentation) were always observed at diakinesis and metaphase I (Figures 6A and 6B), suggesting that breaks are not correctly repaired. In addition, chromosome bridges and fragmentation were observed in anaphase I, resulting in the production of unbalanced meiotic products at telophase II (Figure 6A) and plant sterility as measured by seed set (Figure 6C).

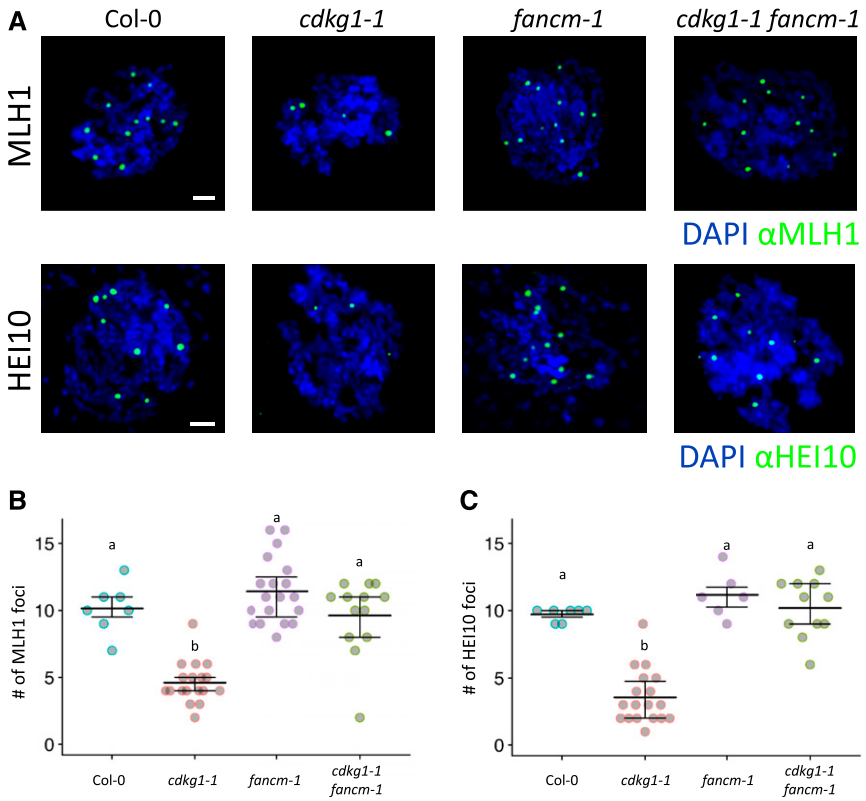

Figure 5. Class I CO Formation Is Restored in the *cdkg1-1 fancm-1* Double Mutant.

(A) Immunolocalization of the class I CO marker proteins (green) MLH1 (top panel) and HEI10 (bottom panel) in diplotene nuclei of Col-0, *cdkg1-1*, *fancm-1*, and *cdkg-1-1 fancm-1* mutant plants. DNA is counterstained with DAPI (blue). Images represent maximum projections of Z-stacks. Bar = 2 μm.
(B) and **(C)** Number of MLH1 **(B)** and HEI10 **(C)** foci observed in the indicated mutants. Graphs show mean and interquartile range as well as the actual foci counts. Superscript letters indicate the significance groups for $P < 0.001$, calculated using ANOVA, with post hoc pairwise *t* tests using nonpooled SD and Bonferroni correction.

To confirm that the aberrant recombination intermediates in a *cdkg1-1 fancm-1* double mutant occur via class II pathways rather than the class I pathway, we produced a triple *cdkg1-1 fancm-1 msh5-2* mutant. As can be seen in Figure 7 and as has been previously reported by Crismani et al. (2012), the *fancm-1* mutation restores bivalent formation and fertility in a *msh5-2* mutant. However, in the triple *cdkg1-1 fancm-1 msh5-2* mutant, recombination intermediates are not correctly resolved, resulting in the formation of chromosome aggregates at metaphase I, linkage between chromosomes, and chromosome breakage at anaphase I (Figures 7A and 7B). Thus, the meiotic behavior of the triple mutant mirrors that of the *cdkg1-1 fancm-1* double mutant, and like the double *cdkg1-1 fancm-1* mutant the triple mutants are sterile (Figure 7C). These results indicate that events leading to metaphase I chromosome aggregates occur when both CDKG1 and FANCM are absent and are independent of the status of the class I CO pathway.

CDKG1 Is Necessary for HR in Somatic Tissues

Our data suggest that CDKG1 is required for progression of the major recombination pathways in meiotic cells, raising the possibility that, like many other proteins (e.g., FANCM and RECQ4; Hartung et al., 2006; Knoll and Puchta, 2011), it plays a similar role in somatic cells. To test whether CDKG1 was also necessary for DNA repair in somatic cells, we crossed the *cdkg1-1* mutant with the HR reporter line IC9 (Molinier et al., 2004). When DNA damage is induced by genotoxic agents, those lesions repaired through the HR pathway are detected by the presence of blue sectors in the IC9 line. In untreated plants, the number of spontaneous recombination events is significantly reduced in the *cdkg1-1* mutant compared to the control IC9 line (0.5 ± 0.1 sectors in the IC9 line versus 0.2 ± 0.1 sectors in the IC9 *cdkg1-1*; $P < 0.001$; Figure 8A). In addition, the rate of HR DNA repair in the *cdkg1-1* mutant was significantly reduced when plants were treated with bleomycin (from 19.2 ± 10.3 to 4.2 ± 3.0 blue sectors per plant; $P < 0.001$) and cisplatin treatments (from 20.6 ± 9.2 to 2 ± 3.4 blue sectors per plant; $P < 0.001$; Figures 8B and 8C). Surprisingly, *cdkg1-1* plants, like Col-0 plants, were sensitive to root growth inhibition by bleomycin in contrast to the *sog-1* mutant, which fails to respond to DNA damage and is less sensitive to root growth inhibition by bleomycin (Figure 8D; Yoshiyama et al., 2009). This suggests that most DNA breaks are repaired by a non–HR-dependent pathway. In support of this, we

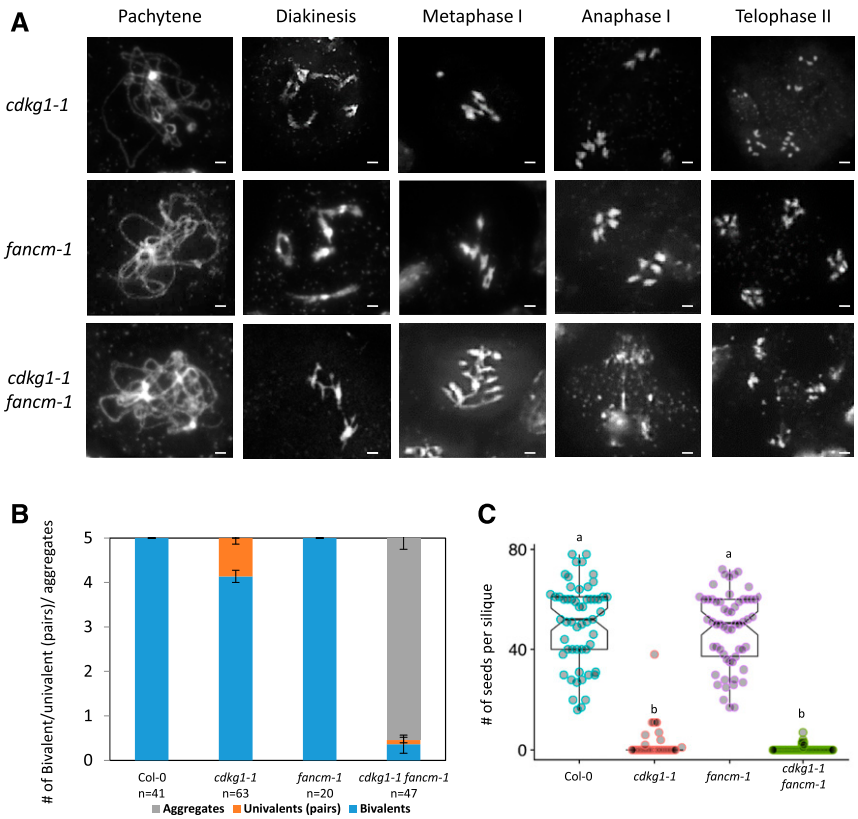

Figure 6. CDKG1 Is Necessary for the Resolution of Recombination Intermediates in the *fancm-1* Mutant.

(A) DAPI-stained chromosome spreads of different meiotic stages in the *cdkg1-1*, *fancm-1*, and *cdkg1-1 fancm-1* mutant as indicated. While in the single mutant five bivalents are observed at metaphase I, in the double mutant chromosome aggregates are present at metaphase I and chromosome bridges observed at anaphase I. Bar = 2 μm.

(B) Ratio of bivalent, univalent pairs and chromosome aggregates present at metaphase I. Error bars represent average ± SD, and *n* indicates the number of metaphases counted for each genotype.

(C) Fertility counts in the indicated mutants. Graphs show mean and interquartile range as well as the actual seed counts. For each genotype at least 30 siliques from three independent plants were counted. Superscript letters indicate the significance groups for $P < 0.001$, calculated using ANOVA, with post hoc pairwise *t* tests using nonpooled SD and Bonferroni correction.

observed that the expression of genes involved in the HR pathway including *RAD51*, is not altered in the *cdkg1-1* mutant compared to the wild type Col-0 (Figure 8E), while in the DNA repair-deficient mutant *atm-1* expression of these genes is not induced in response to bleomycin treatment (Figure 8E; Garcia et al., 2003; Cimprich and Cortez, 2008; Culligan and Britt, 2008).

Taken together, these data suggest that CDKG1 has a global role in HR-based DNA repair in somatic and meiotic cells promoting the orderly progression of canonical HR pathways.

DISCUSSION

Cyclin-dependent kinases and their cognate cyclins have been shown to have important roles during meiosis and recombination in many organisms (Trovesi et al., 2013; Gómez-Escoda and Wu, 2017; Wijnker et al., 2019; Yang et al., 2020). We have previously demonstrated that CDKG1 is necessary for CO formation and homologous chromosome synapsis at high ambient temperature during male meiosis in Arabidopsis (Zheng et al., 2014). Here, we describe a role for CDKG1 in the stabilization of meiotic and somatic recombination intermediates.

CDKG1 Promotes the Stability of Early Recombination Intermediates

In the *cdkg1-1* mutant, early events such as DSB formation and the loading of the strand invasion and exchange proteins RAD51 and DMC1 were found to be normal (Zheng et al., 2014). Despite this, synapsis and CO formation were drastically reduced, suggesting that CDKG1 acts downstream of these early recombination events. After strand invasion and D-loop stabilization, ~100 sites are designated as potential class I COs and marked by the presence of ZMM proteins, including HEI10. As prophase progresses, the number of HEI10 foci decreases, until by late pachytene all remaining HEI10 foci colocalize with MLH1 and mark sites of future class I COs (Chelysheva et al., 2012). In the absence of the ZMM protein MSH5, class I COs are not formed, and the recombination intermediates are resolved as NCOs, resulting in

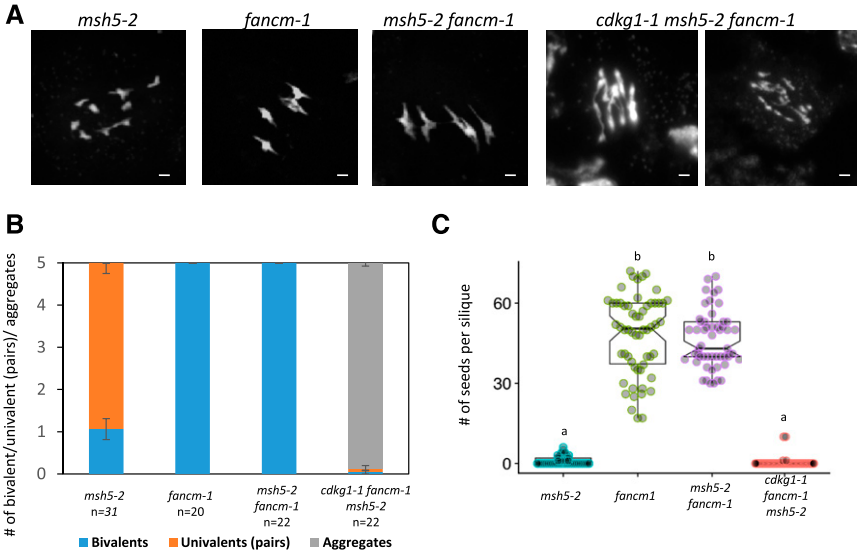

Figure 7. In the Absence of CDKG1, the *fancm-1* Mutation Is Not Able to Rescue the *msh5-2* Phenotype.

(A) DAPI-stained metaphase I spreads. Bar = 2 μm.

(B) Ratio of bivalent, univalent pairs and chromosome aggregates present at metaphase I. Error bars represent average ± SD, and *n* indicates the number of metaphases counted for each genotype.

(C) Fertility counts in the indicated mutants. Graphs show mean and interquartile range as well as the actual seed counts. For each genotype at least 30 siliques from three independent plants were counted. Superscript letters indicate the significance groups for $P < 0.001$, calculated using ANOVA, with post hoc pairwise *t* tests using nonpooled SD and Bonferroni correction.

the presence of univalents at metaphase I and consequent sterility (Higgins et al., 2008b; Lu et al., 2008). Unexpectedly, we observed increased CO number and seed set in the double *cdkg1-1 msh5-2* mutant compared to the single *msh5-2* mutant. As the class I CO pathway is defective in the double mutant, the extra COs must come from a ZMM-independent pathway. The presence of additional class II COs in both the single *cdkg1-1* and the double *cdkg1-1msh5-2* mutant is also supported by the results obtained when bivalent distributions were simulated. While for the single *msh5-2* mutant the best fit bivalent number was obtained for 1.16 class II COs per meiosis, for the *cdkg1-1* and *cdkg1-1 msh5-2* mutants the best fit was observed for 3.76 and 3.41 class II COs, respectively, per meiosis. In yeast, mutations of the early recombination protein MLH2 and its interacting partner Mer3 also improve spore viability of *msh4* mutants, and the authors suggest that this might be due to an increased capacity of the double mutants to make COs (Duroc et al., 2017). Indeed, the double *msh4mlh2* and *msh5mlh2* mutants show increased CO frequency over specific genetic intervals (Abdullah et al., 2004). The MLH1-Mer3 complex preferentially recognizes D-loops and DNA branched structures, and it is thought to act by stopping D-loop extension (Duroc et al., 2017). Furthermore, this activity seems to be independent of the fate of the D-loop intermediates, akin to what we observe in the *cdkg1-1* mutant.

Where then do these additional class II COs come from? One possibility is that in the absence of CDKG1, a number of the recombination intermediates that would normally be destined for the class I pathway are repaired via the DSB processing pathways operating in parallel. In the wild type, of the ~200 DSBs initiated in early prophase (Chelysheva et al., 2012; Choi et al., 2013; Girard et al., 2015; Séguéla-Arnaud et al., 2015) approximately half are thought to be processed by the ZMM proteins (Higgins et al., 2004, 2008a; Chelysheva et al., 2012), with the remaining breaks processed by parallel non-ZMM pathways, for example, via MUS81 or FANCD2 (Figure 9; Kurzbauer et al., 2018). A small percentage of the joint molecules processed by these secondary pathways are eventually resolved as class II COs (Mercier et al., 2015). Channelling more intermediates through non-ZMM pathways in a *cdkg1-1* mutant could therefore result in additional class II COs, together with an equivalent decrease in the number of stable early class I intermediates (Figure 9). This possibility is directly supported by our observation of reduced HEI10 foci during leptotene in the *cdkg1-1* mutant, indicating fewer DSBs being processed by the ZMM proteins in the absence of CDKG1. Given that the wild-type numbers of DSBs occur in a *cdkg1-1* mutant (Zheng et al., 2014), a large number of intermediates that would normally be processed by ZMM proteins in the wild type must be processed by other pathways in a *cdkg1-1* mutant (Figure 9). Another possible explanation is that in the absence of CDKG1, joint molecules that enter the class II pathways have a greater likelihood of being repaired as COs. In either situation, the recombination intermediates are processed by a MUS81-independent pathway, likely involving FANCD2 (Kurzbauer et al., 2018), as the double *cdkg1-1mus81-2* mutant behaves as the single *cdkg1-1* mutant.

A greater reliance on the DSB processing pathways that operate in parallel to the class I CO pathway is also suggested by the presence of chromosome aggregates at metaphase in a *cdkg1-1 fancm-1* double mutant. The helicase FANCM is an integral component of the meiotic DSB processing machinery and promotes dissolution of joint molecules that have the potential to

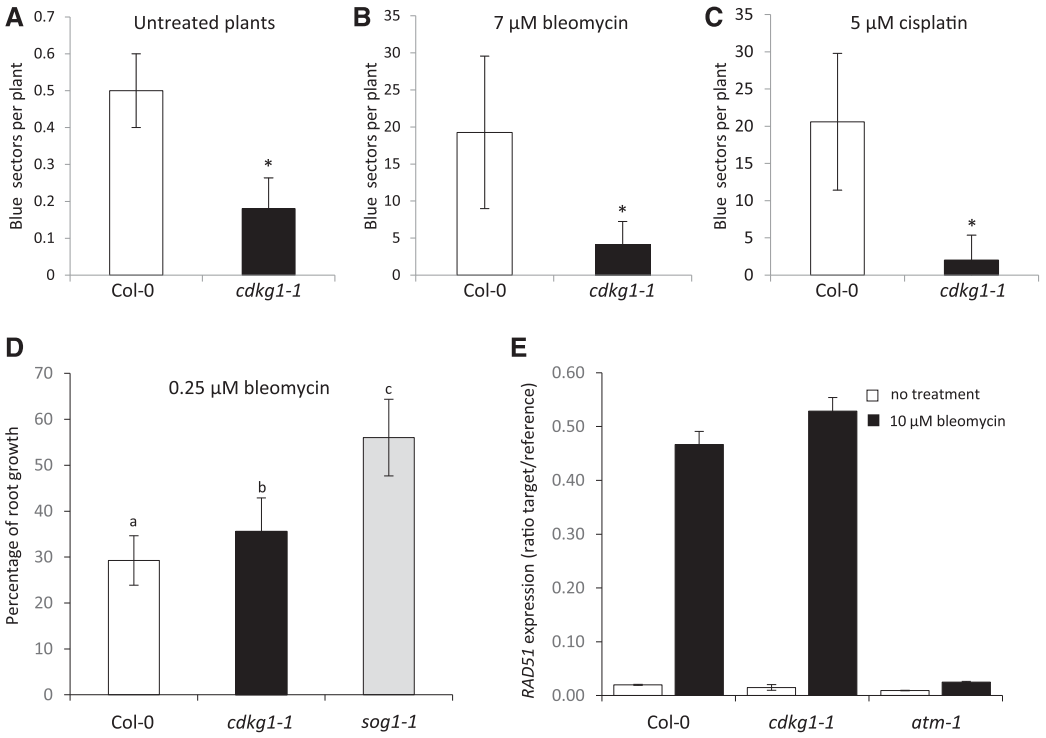

Figure 8. Rates of Somatic HR Are Reduced in the *cdkg1-1* Mutant.

(A) Spontaneous recombination rates in Col-0 and the *cdkg1-1* mutant. Graphs represent averages ± SD for 10 plants. Asterisks indicate values that are significantly different for $P < 0.001$, using two-tailed *t* test.

(B) and **(C)** Recombination rates for Col-0 and the *cdkg1-1* mutant in the presence of 7 μM bleomycin **(B)** or 5 μM cisplatin **(C)**. Graphs represent averages ± SD for 10 plants.

(D) Percentage of root growth in media containing 0.25 μM bleomycin for Col-0, *cdkg1-1*, and *sog1-1* seedlings compared with growth in media with no bleomycin. Graphs represent averages ± SD for thirty 8-d-old seedlings. Superscript letters indicate the significance groups for $P < 0.001$ calculated using ANOVA, with post hoc pairwise *t* tests using nonpooled SD and Bonferroni correction.

(E) Expression of the HR repair pathway gene *RAD51* in Col-0, the *cdkg1-1* mutant, and *atm-1* control 8-d-old seedlings, treated or not with 10 μM bleomycin for 3 h, as determined by qPCR.

become class II COs, diverting them toward NCO or inter-sister repair. One interpretation of the observed chromosome aggregates in a double *cdkg1-1 fancm-1* mutant (but not the respective single mutants) is that aberrant joint molecules form in the absence of CDKG1 and that FANCM is required to resolve these toxic recombination intermediates. The reciprocal interpretation is also possible, that is, that aberrant joint molecules form in the absence of FANCM that require CDKG1 for resolution. Further experimentation will be required to distinguish between these (or other) possibilities.

Elevated Numbers of Recombination Intermediates Restore Synapsis in the *cdkg1-1* Mutant

Despite the chromosome abnormalities present at metaphase I, full homologous chromosome synapsis is observed in the double *cdkg1-1 fancm-1* mutant. One of the main consequences of a *fancm* mutation is the persistence of a large number of recombination intermediates. In the absence of CDKG1, these recombination intermediates are able to act as synaptic initiation sites resulting in full synapsis in the *cdkg1-1 fancm-1* mutant. By extension, this implies that the synapsis defect in a *cdkg1-1* mutant is due to a deficit in the number of recombination intermediates able to act as synaptic initiation sites, rather than a problem in SC assembly or maintenance.

In some organisms, such as budding yeast, CO formation is necessary for full synapsis to occur (Zickler and Kleckner, 2016) but, in Arabidopsis, after the early recombination events, the SC is able to form even in the absence of ZMM proteins and consequently reduced CO formation (Higgins et al., 2004, 2008b; Mercier et al., 2005; Jackson et al., 2006; Macaisne et al., 2008; Chelysheva et al., 2012), while defects in DSB formation, strand invasion, and D-loop formation and stabilization do lead to incomplete synapsis in Arabidopsis as illustrated by the *dmc1*, *atrad51*, and *atxrcc3* mutants (Couteau et al., 1999; Bleuyard and White, 2004; Li et al., 2004). One possible explanation for this difference is that plants have long chromosomes containing numerous synapsis initiation sites that are not CO-designated sites so loss of COs would have less effect on SC nucleation and polymerization (Zickler and Kleckner, 2016). This could help explain the phenotype of the single *cdkg1-1* mutant. In the single *cdkg1-1* mutant, the number of SICs is reduced, possibly due to

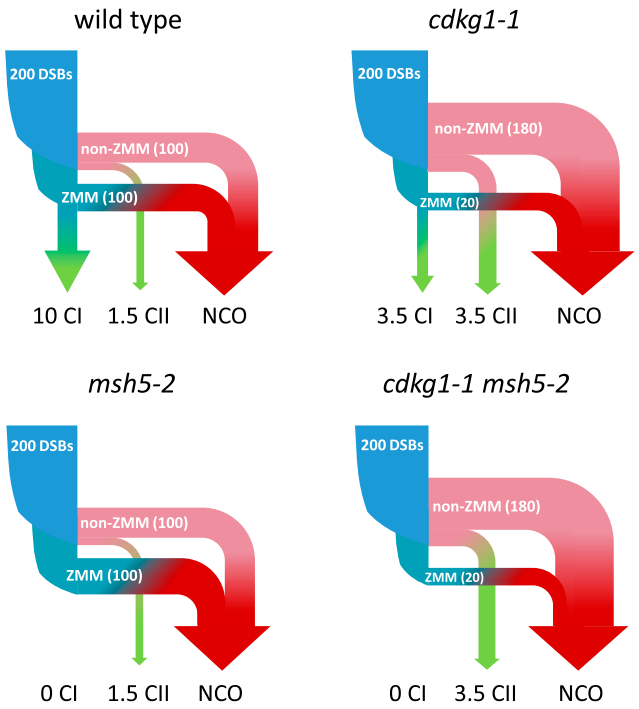

Figure 9. A Model for the Impact of *cdkg1-1* and *msh5-2* Mutations on the Class I (CI) CO, Class II (CII) CO, and Non-crossover (NCO) Pathways in Arabidopsis.

Arrow thickness relates to the proportion of the initial DSBs going through each pathway. Numbers indicate the number of DSBs channeled to each pathway. DSBs: ~200 DMC1/RAD51/γH2AX foci are observed in early meiotic prophase (Choi et al., 2013; Girard et al., 2015; Séguéla-Arnaud et al., 2015; Xue et al., 2018). ZMM intermediates: ~100 MSH4/MSH5/HEI10 foci are observed in the wild-type leptotene/zygotene (Higgins et al., 2004, 2008a; Chelysheva et al., 2012). In *cdkg1-1*, we observe ~20 HEI10 foci in leptotene/zygotene. CI, class I CO.

the reduced stability of recombination intermediates, resulting in fewer HEI10 foci in leptotene, incomplete synapsis, and consequently reduced numbers of class I COs.

In the *cdkg1-1 fancm-1* mutant, more recombination intermediates are maintained and can act as SIC sites. This is in agreement with synapsis initiation occurring early in plants, at the time of strand exchange and D-loop formation.

The Localization of Class I CO Markers Is Restored in a Double *cdkg1-1 fancm-1* Mutant

In addition to the recovery of synapsis in the double *cdkg1-1 fancm-1* mutant, there is also recovery of class I CO events as marked by the presence of HEI10 and MLH1. The recovery of HEI10 foci early in leptotene and zygotene and the normal levels of HEI10 and MLH1 foci at pachytene and diplotene suggest normal numbers of recombination intermediates can be processed by the ZMM pathway in the absence of both CDKG1 and FANCM. How the lack of FANCM restores the ZMM pathway when CDKG1 is absent is unclear. One possibility is that CDKG1 normally protects ZMM intermediates from dissolution by FANCM and that in the absence of both proteins these intermediates persist. Another possibility is that the additional class II CO sites, due to the *fancm-1* mutation, may stabilize inter-homologue associations allowing ZMM intermediates to persist.

Despite the fact that normal levels of ZMM-associated foci are observed during pachytene and diplotene in *cdkg1-1 fancm-1* double mutants, it is not possible to ascertain whether these sites mature as full CO events, as chromosome entanglements are observed at metaphase I. Unresolved ZMM intermediates are not required for the formation of chromosome aggregates, however, as aggregates are also observed in a *cdkg1-1 fancm-1 msh5-2* triple mutant, where class I COs and their precursors are absent. The chromosome aggregate phenotype is reminiscent of that observed in *fancm-1 mus81-2* double mutants (Crismani et al., 2012). In this mutant, unresolved class II recombination intermediates persist, leading to the formation of chromosome entanglements at metaphase I (Crismani et al., 2012). MUS81 has a well-described role in the resolution of Holliday junctions (Osman et al., 2003), and there is also support for CDKs having a role in CO maturation (Palmer et al., 2019).

In wheat–rye (*Secale cereale*) hybrids, which possess no true homologous chromosomes, only an average of 0.58 chiasmata per cell are observed at metaphase I, despite an average of ~20 MLH1 foci being observed at diplotene (Martín et al., 2014). In this context, the ability of the MLH1 marked foci to mature as chiasmata is suppressed by the *Ph1* locus, which contains a cluster of defective CDKs closely related to the CDKG group in Arabidopsis (Griffiths et al., 2006; Zheng et al., 2014). *Ph1* is thought to negatively regulate CDK activity, leading the authors to suggest that CDK activity promotes maturation of MLH1 sites in wheat–rye hybrids (Martín et al., 2014).

A Wider Role for CDKG1 in Recombination Pathways in Arabidopsis

Our data indicate that in addition to its meiotic role, CDKG1 is also involved in somatic DNA repair. In the absence of CDKG1, we observed a reduction in the rate of HR DNA repair after spontaneous and induced DNA lesions. This reduction occurred after treatment with bleomycin, which induces DSBs, and also with cisplatin, which is thought to cause DNA cross-links (Brabec, 2002), suggesting that CDKG1 promotes DNA repair from both types of lesions. This contrasts with what is observed for FANCM and RECQ4A mutants. While FANCM is required for DSB-induced DNA repair, it suppresses spontaneous and cisplatin-induced HR (Knoll et al., 2012). RECQ4A, on the other hand, is thought to suppress the repair of defects arising during DNA replication and not the ones caused by DSB formation (Hartung et al., 2006). These observations again suggest that CDKG1 is important during the early stages of DNA repair, likely by helping to stabilize recombination intermediates, and show that CDKG1 acts independently of other anti-CO proteins during the recombination process. Although HR DNA repair was reduced in the *cdkg1-1* mutant, we did not observe increased sensitivity to genotoxic agents or altered expression of DNA repair genes, indicating that despite the fact that HR is suppressed in the *cdkg1-1* mutant, DNA damage is still repaired via alternative pathways.

A Model for the Role of CDKG1 during Male Meiosis

Our data indicate that CDKG1 is important for the formation and/or stabilization of both meiotic and somatic recombination intermediates. In the *cdkg1-1* mutant, the stability of early recombination intermediates normally processed by the class I CO pathway is compromised, resulting in reduced HEI10 foci in leptotene and zygotene, reduced synapsis, and decreased levels of class I COs. As DSB formation appears normal in a *cdkg1-1* mutant, our results suggest that the DSBs not captured by the class I recombination pathway are processed by parallel DNA repair pathways. This is accompanied by the formation of additional class II COs in both the presence and absence of an otherwise functioning ZMM pathway (Figure 9). This contrasts with what is observed in ZMM mutants, where recombination intermediates destined to be processed by the ZMM proteins are resolved as NCOs. We suggest therefore that CDKG1 acts upstream of the ZMM proteins and helps stabilize or maintain intermediates for processing by the ZMM recombination pathway.

In addition to its meiotic role, it is clear that CDKG1 also has wider functions including the role in promoting somatic DNA repair by HR described here. Moreover, CDKG1 affects splicing in somatic tissues (Cavallari et al., 2018), and in anthers, the loss of CDKG1 results in the incorrect splicing of the callose synthase gene *CalS5*, impaired callose synthesis, and abnormal pollen cell wall formation (Huang et al., 2013). This likely contributes to the low seed set observed in *cdkg1-1* mutants, despite a relatively modest reduction in bivalent number. While the possibility that CDKG1 fine-tunes recombination outcomes during male meiosis by regulating the splicing of meiotic genes is an attractive hypothesis, alternative possibilities include the direct phosphorylation of meiotic proteins or their immediate regulators, leading to changes in activity or levels. However, the underlying molecular mechanisms remain obscure and merit further investigation.

METHODS

Plant Material and Growth Conditions

Plants were grown in growth rooms under long-day conditions (16-h-light/8-h-dark cycle, light intensity of 150 μmol m^{-2} s^{-1}, provided by Sylvania 840 lamps) with the temperature set at 23°C. The mutant lines used in this study have previously been described; *cdkg1-1,* SALK_075762; (Zheng et al., 2014), *mus81-2* (SALK_107515; Higgins et al., 2008a), *msh5-2* (SALK_026553; Higgins et al., 2008b), *fancm-1* (Crismani et al., 2012), and IC9 (Molinier et al., 2004). Homozygous lines for each mutant were used for crosses and double and triple mutants identified by PCR-based screening (the full list of primers used for genotyping can be found in Supplemental Table 3). For seed count experiments, all plants were grown at the same time under the same conditions, and at least 30 siliques from three different plants were counted per genotype. Statistical significance was calculated using ANOVA, with post hoc pairwise *t* tests using non-pooled SD and Bonferroni correction (full ANOVA results are given in Supplemental Table 4).

Meiotic Spread Preparation

Whole inflorescences from Col-0 and mutant plants were fixed in 3:1 ethanol:acetic acid and stored at 4°C. Flower buds in the size range 0.3 to 0.9 mm were used to prepare the squashes as described previously (Jenkins and Hasterok, 2007). Slides were then stained with 4′,6-diamidino-2-phenylindole (DAPI) for observation. The bivalent/univalent ratio was determined for at least 20 metaphases per genotype; exact numbers are shown in the respective figures. Statistical significance was calculated using a two-tailed Student's *t* test.

Immunolabeling Arabidopsis Pollen Mother Cells

Meiocites from Col-0 and mutant plants where embedded in acrylamide to preserve their three-dimensional structure and used for the immunolocalization studies as described previously (Phillips et al., 2010), with the following modifications. Buds of Arabidopsis (*Arabidopsis thaliana*) plants in the prophase I meiotic stage (size range, 0.3 to 0.9 mm) were isolated into buffer A and fixed in 2% (w/v) paraformaldehyde for 30 min. After 2 × 10-min washes in buffer A, the buds were macerated with a brass rod in buffer A + 1% (v/v) Lipsol, and the suspension was then embedded in acrylamide. Embedded meiocytes were blocked and incubated with primary antibody solution for 24 to 36 h. The primary antibodies used were α-ASY1 (rat, 1:500; Armstrong et al., 2002), α-ZYP1 (guinea pig, 1:500; Higgins et al., 2005), α-MLH1 (rabbit, 1:250; Chelysheva et al., 2010), and α-HEI10 (rabbit, 1:250; Chelysheva et al., 2012). Secondary antibodies (Alexa Fluor 488 chicken anti-rat [A21470], Alexa Flour 546 donkey anti-rabbit [A10040], and Alexa Flour 633 goat anti–guinea pig [A21105], all from Molecular Probes) were used at 1:500 dilution and incubated overnight. Images were acquired using a TCS SP5II microscope or an SP8 confocal microscope (Leica). Images represent deconvolved maximum projection of Z-stacks. For images obtained with the SP5II microscope, the Z-stacks were deconvolved using AutoQuant ×2 (Media Cybernetics), and for the SP8 microscope using the built-in Lightning software (Leica Microsystems). The same deconvolution parameters were applied for every image. Bivalent tracking and analysis were performed using Imaris 7.3 (Bitplane).

Simulating CO Formation

Meiosis was modeled using the beam-film model of CO patterning (Zhang et al., 2014; White et al., 2017). Parameter values previously determined for the Arabidopsis wild-type male meiosis were applied for each of the five chromosomes (Lloyd and Jenczewski 2019). Class I and class II COs were simulated independently for 10,000 bivalents for each of the five chromosomes and then combined to obtain final CO positions for 10,000 meioses. For each meiosis, the number of bivalents was the number of chromosomes that received at least one CO of either class. The class I CO M value was adjusted to reflect the differing number of MLH1 foci (i.e., class I COs) observed in the respective lines (*msh5-2* and *msh5-2 cdkg1-1*, M = 0, i.e., 100% reduction in class I COs; *cdkg1-1* M = 0.354, i.e., 64.6% reduction in class I COs). The proportion of DSBs that become class II COs (T2Prob) was varied from 30% of wild-type values to 450% of wild-type values, corresponding to a range of 0.5 to 7 class II COs per meiosis. Complete parameter values used in simulations are provided in Supplemental Table 2. Best fit values for class II COs were obtained by comparing the average number of bivalents for each simulation round to the average number of bivalents observed cytologically. P-values were calculated using Bonferroni corrected values derived from two-sample Kolmogorov–Smirnov tests.

HR Assays

HR assays were performed as described previously (Hartung et al., 2007). Briefly, the 7-d-old wild-type Col-0 and *cdkg1-1* mutant seedlings carrying the IC9 reporter construct (Molinier et al., 2004) were transferred to liquid media containing 7 μM bleomycin, 5 μM cisplatin, or solvent control and incubated in the light at 22°C for 8 d. The β-glucuronidase staining reaction was done at 37°C for 2 d, and pigment extraction was done using 70% (v/v)

ethanol. The number of blue sectors per plant was counted under a binocular microscope. For the root growth assays, plants were germinated at 22°C in media containing 0.25 μM bleomycin or solvent control. Root growth was measured after 8 d. For each treatment, 30 seedlings were used, and the experiment repeated three times with similar results. Statistical significance was calculated using ANOVA, with post hoc pairwise *t* tests using nonpooled SD and Bonferroni correction.

qPCR

Total RNA was extracted from seedlings treated with 10 μM bleomycin or solvent control for 3 h using the RNeasy Plant Mini kit (Qiagen). Total mRNA (1 μg) was used to generate cDNA using the SuperScript III First-strand Synthesis kit (Invitrogen). qPCRs were performed using the LightCycler 480 system (Roche). Typically, 10 ng of cDNA was used in a 20 μL reaction containing 0.25 μM of each primer and 10 μL of LightCycler 480 SYBR Green I Master. Each sample was analyzed in triplicate using *Rad51*-specific primers as described by Wang et al. (2014), and *Actin2* expression was used as a reference (Supplemental Table 3). Data were analyzed using the LightCycler 480 software.

Accession Numbers

Sequence data from this article can be found in the GenBank/EMBL data libraries under accession numbers CDKG1 (At5g63370), MSH5 (At3g20475), MUS81 (At4g30870), and FANCM (At1g35530).

Supplemental Data

Supplemental Figure 1. Equivalent numbers of class II COs are modeled for *cdkg1-1* and *cdkg1-1 msh5-2*.

Supplemental Figure 2. HEI10 localization in leptotene, zygotene, pachytene and diplotene nuclei of Col-0, *cdkg1-1*, *fancm-1* and *cdkg-1-1 fancm-1* mutant plants as indicated.

Supplemental Table 1. Comparisons of experimental and simulated bivalent distributions.

Supplemental Table 2. Parameter values used in beam-film simulations.

Supplemental Table 3. List of primers used in this study.

Supplemental Table 4. Statistical analysis tables.

ACKNOWLEDGMENTS

We thank Raphael Mercier for kindly providing the *fancm-1*, *msh5-2*, and *msh5-2 fancm-1* mutants; Holger Puchta for the HR recombination marker IC9 line; and Mathilde Grelon for providing the MLH1 and HEI10 antibodies. Special thanks to Glyn Jenkins, Kim Osman, and Eugenio Sanchez-Moran for many helpful discussions. This work was funded by the Biotechnology and Biological Sciences Research Council (grants BB/M009459/1 and BB/CSP1730/1), by a Marie Curie COFUND grant (663830-AU-110 to A.L.), by the National Science Centre Poland (grant 2014/14/M/NZ2/00519 to A.B.), and by the EU Erasmus+ Programme (to F.T. and D.D.).

AUTHOR CONTRIBUTIONS

C.N., A.L., D.W.P., and J.H.D. designed the experiments; C.N., D.D., A.B., and F.T. performed the experiments; C.N., D.W.P., and A.L. analyzed the data; C.N., A.L., D.W.P., and J.H.D. wrote the article. All authors read and approved the article.

Received December 3, 2019; revised January 22, 2020; accepted February 8, 2020; published February 10, 2020.

REFERENCES

Abdullah, M.F.F., Hoffmann, E.R., Cotton, V.E., and Borts, R.H. (2004). A role for the MutL homologue MLH2 in controlling heteroduplex formation and in regulating between two different crossover pathways in budding yeast. Cytogenet. Genome Res. **107:** 180–190.

Allers, T., and Lichten, M. (2001). Differential timing and control of noncrossover and crossover recombination during meiosis. Cell **106:** 47–57.

Armstrong, S.J., Caryl, A.P., Jones, G.H., and Franklin, F.C.H. (2002). Asy1, a protein required for meiotic chromosome synapsis, localizes to axis-associated chromatin in Arabidopsis and Brassica. J. Cell Sci. **115:** 3645–3655.

Basu-Roy, S., Gauthier, F., Giraut, L., Mézard, C., Falque, M., and Martin, O.C. (2013). Hot regions of noninterfering crossovers coexist with a nonuniformly interfering pathway in *Arabidopsis thaliana*. Genetics **195:** 769–779.

Berchowitz, L.E., Francis, K.E., Bey, A.L., and Copenhaver, G.P. (2007). The role of AtMUS81 in interference-insensitive crossovers in *A. thaliana*. PLoS Genet. **3:** e132.

Bishop, D.K., Park, D., Xu, L., and Kleckner, N. (1992). DMC1: A meiosis-specific yeast homolog of E. coli recA required for recombination, synaptonemal complex formation, and cell cycle progression. Cell **69:** 439–456.

Bleuyard, J.-Y., and White, C.I. (2004). The Arabidopsis homologue of Xrcc3 plays an essential role in meiosis. EMBO J. **23:** 439–449.

Brabec, V. (2002). DNA modifications by antitumor platinum and ruthenium compounds: their recognition and repair. In Progress in Nucleic Acid Research and Molecular Biology, K. Moldave, ed (New York: Academic Press), pp. 1–68.

Cavallari, N., Nibau, C., Fuchs, A., Dadarou, D., Barta, A., and Doonan, J.H. (2018). The cyclin-dependent kinase G group defines a thermo-sensitive alternative splicing circuit modulating the expression of Arabidopsis ATU2AF65A. Plant J. **94:** 1010–1022.

Chelysheva, L., Grandont, L., Vrielynck, N., le Guin, S., Mercier, R., and Grelon, M. (2010). An easy protocol for studying chromatin and recombination protein dynamics during *Arabidopsis thaliana* meiosis: Immunodetection of cohesins, histones and MLH1. Cytogenet. Genome Res. **129:** 143–153.

Chelysheva, L., Vezon, D., Chambon, A., Gendrot, G., Pereira, L., Lemhemdi, A., Vrielynck, N., Le Guin, S., Novatchkova, M., and Grelon, M. (2012). The Arabidopsis HEI10 is a new ZMM protein related to Zip3. PLoS Genet. **8:** e1002799.

Choi, K., Zhao, X., Kelly, K.A., Venn, O., Higgins, J.D., Yelina, N.E., Hardcastle, T.J., Ziolkowski, P.A., Copenhaver, G.P., Franklin, F.C.H., McVean, G., and Henderson, I.R. (2013). Arabidopsis meiotic crossover hot spots overlap with H2A.Z nucleosomes at gene promoters. Nat. Genet. **45:** 1327–1336.

Cimprich, K.A., and Cortez, D. (2008). ATR: An essential regulator of genome integrity. Nat. Rev. Mol. Cell Biol. **9:** 616–627.

Colaiácovo, M.P., MacQueen, A.J., Martinez-Perez, E., McDonald, K., Adamo, A., La Volpe, A., and Villeneuve, A.M. (2003). Synaptonemal complex assembly in C. elegans is dispensable for loading strand-exchange proteins but critical for proper completion of recombination. Dev. Cell **5:** 463–474.

Couteau, F., Belzile, F., Horlow, C., Grandjean, O., Vezon, D., and Doutriaux, M.P. (1999). Random chromosome segregation without meiotic arrest in both male and female meiocytes of a dmc1 mutant of Arabidopsis. Plant Cell **11:** 1623–1634.

Couteau, F., Nabeshima, K., Villeneuve, A., and Zetka, M. (2004). A component of *C. elegans* meiotic chromosome axes at the interface of homolog alignment, synapsis, nuclear reorganization, and recombination. Curr. Biol. **14:** 585–592.

Crismani, W., Girard, C., Froger, N., Pradillo, M., Santos, J.L., Chelysheva, L., Copenhaver, G.P., Horlow, C., and Mercier, R. (2012). FANCM limits meiotic crossovers. Science **336:** 1588–1590.

Culligan, K.M., and Britt, A.B. (2008). Both ATM and ATR promote the efficient and accurate processing of programmed meiotic double-strand breaks. Plant J. **55:** 629–638.

Dangel, N.J., Knoll, A., and Puchta, H. (2014). MHF1 plays Fanconi anaemia complementation group M protein (FANCM)-dependent and FANCM-independent roles in DNA repair and homologous recombination in plants. Plant J. **78:** 822–833.

Doonan, J.H., and Kitsios, G. (2009). Functional evolution of cyclin-dependent kinases. Mol. Biotechnol. **42:** 14–29.

Duroc, Y., et al. (2017). Concerted action of the MutLβ heterodimer and Mer3 helicase regulates the global extent of meiotic gene conversion. eLife **6:** e21900.

Fernandes, J.B., et al. (2018). FIGL1 and its novel partner FLIP form a conserved complex that regulates homologous recombination. PLoS Genet. **14:** e1007317.

Garcia, V., Bruchet, H., Camescasse, D., Granier, F., Bouchez, D., and Tissier, A. (2003). AtATM is essential for meiosis and the somatic response to DNA damage in plants. Plant Cell **15:** 119–132.

Girard, C., Chelysheva, L., Choinard, S., Froger, N., Macaisne, N., Lehmemdi, A., Mazel, J., Crismani, W., and Mercier, R. (2015). AAA-ATPase FIDGETIN-LIKE 1 and Helicase FANCM antagonize meiotic crossovers by distinct mechanisms. PLoS Genet. **11:** e1005448.

Girard, C., Crismani, W., Froger, N., Mazel, J., Lemhemdi, A., Horlow, C., and Mercier, R. (2014). FANCM-associated proteins MHF1 and MHF2, but not the other Fanconi anemia factors, limit meiotic crossovers. Nucleic Acids Res. **42:** 9087–9095.

Gómez-Escoda, B., and Wu, P.J. (2017). Roles of CDK and DDK in genome duplication and maintenance: meiotic singularities. Genes (Basel) **8:** 105.

Gray, S., and Cohen, P.E. (2016). Control of meiotic crossovers: From double-strand break formation to designation. Annu. Rev. Genet. **50:** 175–210.

Greer, E., Martín, A.C., Pendle, A., Colas, I., Jones, A.M.E., Moore, G., and Shaw, P. (2012). The Ph1 locus suppresses Cdk2-type activity during premeiosis and meiosis in wheat. Plant Cell **24:** 152–162.

Griffiths, S., Sharp, R., Foote, T.N., Bertin, I., Wanous, M., Reader, S., Colas, I., and Moore, G. (2006). Molecular characterization of Ph1 as a major chromosome pairing locus in polyploid wheat. Nature **439:** 749–752.

Hartung, F., Suer, S., Bergmann, T., and Puchta, H. (2006). The role of AtMUS81 in DNA repair and its genetic interaction with the helicase AtRecQ4A. Nucleic Acids Res. **34:** 4438–4448.

Hartung, F., Suer, S., and Puchta, H. (2007). Two closely related RecQ helicases have antagonistic roles in homologous recombination and DNA repair in *Arabidopsis thaliana*. Proc. Natl. Acad. Sci. USA **104:** 18836–18841.

Higgins, J.D., Armstrong, S.J., Franklin, F.C.H., and Jones, G.H. (2004). The Arabidopsis MutS homolog AtMSH4 functions at an early step in recombination: evidence for two classes of recombination in Arabidopsis. Genes Dev. **18:** 2557–2570.

Higgins, J.D., Buckling, E.F., Franklin, F.C.H., and Jones, G.H. (2008a). Expression and functional analysis of AtMUS81 in Arabidopsis meiosis reveals a role in the second pathway of crossing-over. Plant J. **54:** 152–162.

Higgins, J.D., Sanchez-Moran, E., Armstrong, S.J., Jones, G.H., and Franklin, F.C.H. (2005). The Arabidopsis synaptonemal complex protein ZYP1 is required for chromosome synapsis and normal fidelity of crossing over. Genes Dev. **19:** 2488–2500.

Higgins, J.D., Vignard, J., Mercier, R., Pugh, A.G., Franklin, F.C.H., and Jones, G.H. (2008b). AtMSH5 partners AtMSH4 in the class I meiotic crossover pathway in *Arabidopsis thaliana*, but is not required for synapsis. Plant J. **55:** 28–39.

Housworth, E.A., and Stahl, F.W. (2003). Crossover interference in humans. Am. J. Hum. Genet. **73:** 188–197.

Huang, X.-Y., Niu, J., Sun, M.-X., Zhu, J., Gao, J.-F., Yang, J., Zhou, Q., and Yang, Z.-N. (2013). CYCLIN-DEPENDENT KINASE G1 is associated with the spliceosome to regulate CALLOSE SYNTHASE5 splicing and pollen wall formation in Arabidopsis. Plant Cell **25:** 637–648.

Hurel, A., Phillips, D., Vrielynck, N., Mézard, C., Grelon, M., and Christophorou, N. (2018). A cytological approach to studying meiotic recombination and chromosome dynamics in *Arabidopsis thaliana* male meiocytes in three dimensions. Plant J. **95:** 385–396.

Jackson, N., Sanchez-Moran, E., Buckling, E., Armstrong, S.J., Jones, G.H., and Franklin, F.C.H. (2006). Reduced meiotic crossovers and delayed prophase I progression in AtMLH3-deficient Arabidopsis. EMBO J. **25:** 1315–1323.

Jang, J.K., Sherizen, D.E., Bhagat, R., Manheim, E.A., and McKim, K.S. (2003). Relationship of DNA double-strand breaks to synapsis in Drosophila. J. Cell Sci. **116:** 3069–3077.

Jenkins, G., and Hasterok, R. (2007). BAC 'landing' on chromosomes of *Brachypodium distachyon* for comparative genome alignment. Nat. Protoc. **2:** 88–98.

Keeney, S., Giroux, C.N., and Kleckner, N. (1997). Meiosis-specific DNA double-strand breaks are catalyzed by Spo11, a member of a widely conserved protein family. Cell **88:** 375–384.

Knoll, A., Higgins, J.D., Seeliger, K., Reha, S.J., Dangel, N.J., Bauknecht, M., Schröpfer, S., Franklin, F.C.H., and Puchta, H. (2012). The Fanconi anemia ortholog FANCM ensures ordered homologous recombination in both somatic and meiotic cells in Arabidopsis. Plant Cell **24:** 1448–1464.

Knoll, A., and Puchta, H. (2011). The role of DNA helicases and their interaction partners in genome stability and meiotic recombination in plants. J. Exp. Bot. **62:** 1565–1579.

Kottemann, M.C., and Smogorzewska, A. (2013). Fanconi anaemia and the repair of Watson and Crick DNA crosslinks. Nature **493:** 356–363.

Kurzbauer, M.T., Pradillo, M., Kerzendorfer, C., Sims, J., Ladurner, R., Oliver, C., Janisiw, M.P., Mosiolek, M., Schweizer, D., Copenhaver, G.P., and Schlögelhofer, P. (2018). *Arabidopsis thaliana* FANCD2 promotes meiotic crossover formation. Plant Cell **30:** 415–428.

Lambing, C., Franklin, F.C.H., and Wang, C.R. (2017). Understanding and manipulating meiotic recombination in plants. Plant Physiol. **173:** 1530–1542.

Li, W., Chen, C., Markmann-Mulisch, U., Timofejeva, L., Schmelzer, E., Ma, H., and Reiss, B. (2004). The Arabidopsis AtRAD51 gene is dispensable for vegetative development but required for meiosis. Proc. Natl. Acad. Sci. USA **101:** 10596–10601.

Li, Y., Qin, B., Shen, Y., Zhang, F., Liu, C., You, H., Du, G., Tang, D., and Cheng, Z. (2018). HEIP1 regulates crossover formation during meiosis in rice. Proc. Natl. Acad. Sci. USA **115:** 10810–10815.

Lloyd, A., and Jenczewski, E. (2019). Modelling sex-specific crossover patterning in *Arabidopsis*. Genetics **211:** 847–859.

Lu, X., Liu, X., An, L., Zhang, W., Sun, J., Pei, H., Meng, H., Fan, Y., and Zhang, C. (2008). The Arabidopsis MutS homolog AtMSH5 is required for normal meiosis. Cell Res. **18:** 589–599.

Macaisne, N., Novatchkova, M., Peirera, L., Vezon, D., Jolivet, S., Froger, N., Chelysheva, L., Grelon, M., and Mercier, R. (2008). SHOC1, an XPF endonuclease-related protein, is essential for the formation of class I meiotic crossovers. Curr. Biol. **18:** 1432–1437.

Martín, A.C., Shaw, P., Phillips, D., Reader, S., and Moore, G. (2014). Licensing MLH1 sites for crossover during meiosis. Nat. Commun. **5:** 4580.

Mercier, R., Jolivet, S., Vezon, D., Huppe, E., Chelysheva, L., Giovanni, M., Nogué, F., Doutriaux, M.P., Horlow, C., Grelon, M., and Mézard, C. (2005). Two meiotic crossover classes cohabit in Arabidopsis: One is dependent on MER3, whereas the other one is not. Curr. Biol. **15:** 692–701.

Mercier, R., Mezard, C., Jenczewski, E., Macaisne, N., and Grelon, M. (2015). The molecular biology of meiosis in plants. Annu. Rev. Plant Biol. **66:** 297–327.

Molinier, J., Ries, G., Bonhoeffer, S., and Hohn, B. (2004). Interchromatid and interhomolog recombination in *Arabidopsis thaliana*. Plant Cell **16:** 342–352.

Osman, F., Dixon, J., Doe, C.L., and Whitby, M.C. (2003). Generating crossovers by resolution of nicked Holliday junctions: A role for Mus81-Eme1 in meiosis. Mol. Cell **12:** 761–774.

Palmer, N., Talib, S.Z.A., and Kaldis, P. (2019). Diverse roles for CDK-associated activity during spermatogenesis. FEBS Lett. **593:** 2925–2949.

Phillips, D., Nibau, C., Ramsay, L., Waugh, R., and Jenkins, G. (2010). Development of a molecular cytogenetic recombination assay for barley. Cytogenet. Genome Res. **129:** 154–161.

Séguéla-Arnaud, M., Choinard, S., Larchevêque, C., Girard, C., Froger, N., Crismani, W., and Mercier, R. (2017). RMI1 and TOP3α limit meiotic CO formation through their C-terminal domains. Nucleic Acids Res. **45:** 1860–1871.

Séguéla-Arnaud, M., et al. (2015). Multiple mechanisms limit meiotic crossovers: TOP3α and two BLM homologs antagonize crossovers in parallel to FANCM. Proc. Natl. Acad. Sci. USA **112:** 4713–4718.

Serra, H., Lambing, C., Griffin, C.H., Topp, S.D., Nageswaran, D.C., Underwood, C.J., Ziolkowski, P.A., Séguéla-Arnaud, M., Fernandes, J.B., Mercier, R., and Henderson, I.R. (2018). Massive crossover elevation via combination of *HEI10* and *recq4a recq4b* during *Arabidopsis* meiosis. Proc. Natl. Acad. Sci. USA **115:** 2437–2442.

Sung, P., and Robberson, D.L. (1995). DNA strand exchange mediated by a RAD51-ssDNA nucleoprotein filament with polarity opposite to that of RecA. Cell **82:** 453–461.

Trovesi, C., Manfrini, N., Falcettoni, M., and Longhese, M.P. (2013). Regulation of the DNA damage response by cyclin-dependent kinases. J. Mol. Biol. **425:** 4756–4766.

Wang, K., Wang, M., Tang, D., Shen, Y., Miao, C., Hu, Q., Lu, T., and Cheng, Z. (2012). The role of rice HEI10 in the formation of meiotic crossovers. PLoS Genet. **8:** e1002809.

Wang, Y., Xiao, R., Wang, H., Cheng, Z., Li, W., Zhu, G., Wang, Y., and Ma, H. (2014). The Arabidopsis RAD51 paralogs RAD51B, RAD51D and XRCC2 play partially redundant roles in somatic DNA repair and gene regulation. New Phytol. **201:** 292–304.

Whitby, M.C. (2010). The FANCM family of DNA helicases/translocases. DNA Repair (Amst.) **9:** 224–236.

White, M.A., Wang, S., Zhang, L., and Kleckner, N. (2017). Quantitative modeling and automated analysis of meiotic recombination. Methods Mol. Biol. **1471:** 305–323.

Wijnker, E., Harashima, H., Müller, K., Parra-Nuñez, P., de Snoo, C.B., van de Belt, J., Dissmeyer, N., Bayer, M., Pradillo, M., and Schnittger, A. (2019). The Cdk1/Cdk2 homolog CDKA;1 controls the recombination landscape in *Arabidopsis*. Proc. Natl. Acad. Sci. USA **116:** 12534–12539.

Xue, M., Wang, J., Jiang, L., Wang, M., Wolfe, S., Pawlowski, W.P., Wang, Y., and He, Y. (2018). The number of meiotic double-strand breaks influences crossover distribution in Arabidopsis. Plant Cell **30:** 2628–2638.

Yang, C., et al. (2020). The Arabidopsis Cdk1/Cdk2 homolog CDKA;1 controls chromosome axis assembly during plant meiosis. EMBO J. **39:** e101625.

Yoshiyama, K., Conklin, P.A., Huefner, N.D., and Britt, A.B. (2009). Suppressor of gamma response 1 (SOG1) encodes a putative transcription factor governing multiple responses to DNA damage. Proc. Natl. Acad. Sci. USA **106:** 12843–12848.

Zhang, L., Liang, Z., Hutchinson, J., and Kleckner, N. (2014). Crossover patterning by the beam-film model: analysis and implications. PLoS Genet. **10:** e1004042.

Zheng, T., Nibau, C., Phillips, D.W., Jenkins, G., Armstrong, S.J., and Doonan, J.H. (2014). CDKG1 protein kinase is essential for synapsis and male meiosis at high ambient temperature in *Arabidopsis thaliana*. Proc. Natl. Acad. Sci. USA **111:** 2182–2187.

Zickler, D. (2006). From early homologue recognition to synaptonemal complex formation. Chromosoma **115:** 158–174.

Zickler, D., and Kleckner, N. (2016). A few of our favorite things: Pairing, the bouquet, crossover interference and evolution of meiosis. Semin. Cell Dev. Biol. **54:** 135–148.